Reaction Layer Imaging Using Fluorescence Electrochemical Microscopy

Minjun Yang[1], Christopher Batchelor-McAuley[1], Enno Kätelhön[1], Richard G. Compton[1] (✉)

[1] Department of Chemistry, Physical and Theoretical Chemistry Laboratory, University of Oxford, South Parks Road, Oxford OX1 3QZ, United Kingdom

ABSTRACT

The chemical confinement of a pH sensitive fluorophore to a thin-reaction layer adjacent to an electrode surface is explored as potentially innovative route to improving the spatial resolution of fluorescence electrochemical microscopy. A thin layer opto-electrochemical cell is designed, facilitating the visualisation of a carbon fibre (diameter 7.0 um) electrochemical interface. Proton consumption is driven at the interface by the reduction of benzoquinone to hydroquinone and the resulting interfacial pH change is revealed using the fluorophore 8-hydoxypyrene-1,3,6-trisulfonic acid. It is demonstrated that the proton depletion zone may be constrained and controlled by the addition of a finite acid concentration to the system. Simulation of the resulting fluorescence intensity profiles is achieved on the basis of a finite difference model, with excellent agreement between the theoretical and experimental results.

KEYWORDS

Fluorescence electrochemical microscopy, Benzoquinone, pH, Pyranine, Reaction layer, Diffusion

Address correspondence to Richard G. Compton, Richard.compton@chem.ox.ac.uk

Introduction

As a reaction proceeds at an electrochemical interface the concentrations of the species adjacent to the surface are altered from that of the bulk solution. Assuming the experimental setup contains sufficient supporting electrolyte and in the absence of convective effects, then the mass-transport to and from the interface is described by the diffusion equation. The region over which the concentrations of the electroactive species are altered is termed the diffusion layer. The extent of this diffusion layer is ~$(\pi Dt)^{0.5}$, where D is the diffusion coefficient (m^2 s^{-1}) of the species and t is the experimental time (s). [1] In an aqueous room temperature system after only one second the diffusion layer thickness is commonly of the order of tens of microns. Compression of this layer may be achieved simply by studying the reaction at shorter times; however, this is not always experimentally appropriate or desirable. An alternative method for contracting the diffusion layer involves the use of coupled homogeneous solution phase reactions. Here the concentration of a species is constrained to a thin zone adjacent to the electrode due to reaction with a species present in bulk solution. The region over which the species is confined is known as the reaction layer [2] and has dimensions less than that of the diffusion layer.

A prime and excellent example of the use of a reaction layer at an electrochemical interface is found in work originally arising from Xiamen University.[3,4] Here an etchant (bromine for example) is produced at an electrochemical interface. Through the reaction of the etchant with a solution phase scavenger (such as a disulfide), the spatial extent of the produced bromine is limited to a region close to the electrochemical interface.[5] The electrode can subsequently be positioned above a surface and used as a tool to precisely machine structures into the material. This confined etchant layer technique (CELT), which is also referred to in the literature as chemical lensing, [6-8] leads to vastly improved resolution and accuracy of the electrochemical machining approach and has enabled the fabrication of three-dimensional micro- and nanostructures.[3,9 10]

As an imaging methodology fluorescence electrochemical microscopy (FEM) was

first developed in the 1980s;[11] a similar time to the far more widely employed technique of scanning electrochemical microscopy.[12,13] Early FEM studies imaged pH changes at an electrode arising from solvent breakdown.[14,15] Here the pH sensitive dye fluorescein was used in a non-buffered medium to indicate an increase in the pH adjacent to the electrode surface. This work was developed further by Engstrom *et al.* who demonstrated that the technique could be extended more generally to detect pH changes resulting from the reduction of oxygen[16]. Work from the same group also evidenced the release of protons at an interface, these protons arose from oxygen evolution and could be imaged using a fluorescent quinine dye (pk_a = 9.5).[17] The coupling of fluorescent imaging techniques with confocal microscopy by Rudd *et al.* facilitated the visualisation of the pH gradient at a microelectrode in 3D, again fluorescein (10uM) was used to report the local pH.[18,19] This procedure was used to image the activity of a boron doped diamond array[20] and diffusion through a semipermeable membrane.[21] More recently, Kuhn *et al*. have used a similar technique to visualize an electrochemical reaction occurring at a particle under a strong electric field.[22] However, using fluorescein as a pH probe in microscopy experiments has a distinct disadvantage in that both the anionic (pK_a = 4.31, ϕ = 0.37) and dianionic (pK_a = 6.43, ϕ = 0.93) forms of the dye are fluorescent.[23]

The above examples demonstrate cases where FEM has been used to 'indirectly' detect the occurance of an electrochemical reaction (i.e. via a change in the local solution phase pH). Alternately, the direct oxidation or reduction of a fluorescent redox probe may be studied to yield information regarding the reaction rate at the electrochemical interface.[24] Recent work has demonstrated how the dye Nile Red can be confined to an attolitre volume in an oil-in-water emulsion and its dynamic electrochemical behavior monitored optically.[25] Alternately, resazurin (or the structurally related Amplex Red) can be converted electrochemically to the fluorogeic species resorufin. The behavior of this fluorophore reaction has been the focus of a number of studies;[26,27] including, being used to experimentally probe reactions at individual nanoparticles.[28] However, generally for both the indirect and

direct FEM methodologies, when the fluorophore is not confined to a small volume (i.e. it is present in solution) the resolution of the imaging technique is limited by the diffusion of the fluorophore. A notable development in this area is provided in the work of Zhang *et al*. who used the electrochemically formed resorufin as an electrochemical mediator in the oxidation of glucose (an adaption of the vanishing valentine reaction).[27] As a consequence of the coupled solution phase reaction, the fluorophore is confined to a thin reaction layer above the electrode surface, thereby minimising the systems diffusional blurring and avoiding the build-up of the bright fluorophore in the thin layer cell.

This article focuses on the technique of indirect FEM, where a change in pH at the electrochemical interface alters the protonation state and hence adsorption spectrum of a given fluorophore. Here we demonstrate how the technique of chemically confining the fluorophore using a reaction layer can be applied to systems in which the pH is altered at the electrochemical interface. Using the reversible benzoquinone /hydroquinone redox system the pH adjacent to the electrochemical interface is controlled, leading to the deprotonation of the fluorophore 8-hydoxypyrene-1,3,6-trisulfonic acid (HPTS, pyranine). The primary advantage of the use of HPTS for FEM is that in contrast to fluorescein its structure only contains one acidic phenol group (pKa = 7.2). FEM is used to image the electrochemical reaction as a function of the solution phase proton concertation (0.0-0.14 mM). First, the redox benzoquinone/hydroquinone couple is fully experimentally characterized, allowing modelling of the system using finite difference method. This developed theoretical model is based upon a scheme-of-squares, in which the electron transfer and protonation processes as occurring in a step-wise manner, facilitating the successful description of the systems behaviour under low buffering conditions. Second by the study of the fluorophore HPTS, providing thermodynamic data to simulate the concentration profile of all species. Finally, together these species are used to form, control and visualize the proton depletion zone adjacent to an electrode surface. Here we demonstrate the ability of HTPS to be used as a pH indicator in

fluorescence electrochemical microscopy and how its spatial extent can be controlled by alteration of the systems buffering capacity. The resulting simulated concentration profiles as a function of the bulk proton concentration are found to be in excellent agreement with the experimental microscopy results. This work serves to first demonstrate the ability of the use of chemical confinement to alter the reaction layer thickness but also provides a framework upon which future systems can be studied.

Experimental

Chemicals

All chemicals used were of analytical grade and were purchased from Sigma-Aldrich. These chemicals were used without further purification. Aqueous solutions were made using ultrapure water (Millipore, resistivity not less than 18.2 MΩ cm at 25^{o}C). Nitrogen gas (99.998%, BOC Gases plc, Guildford UK) was used to de-oxygenate the electrolytic solutions for 15 minutes prior to experimentation.

Buffer solutions

The buffers contained the following mixture of solutions shown in Table 1. As indicated in the Table the final volume of the citric and potassium phosphate dibasic buffers were adjusted to 100mL with deionized water. However, the final volume of the sodium phosphate mono- and dibasic buffers (PB), and sodium carbonate and dicarbonate buffers were adjusted to 200mL with additional deionized water. The buffer solutions were adjusted to the precise pH values indicated using small amounts of 1M HCl/NaOH. This adjustment was done via measurement with a pH 213 microprocessor pH meter (HANNA Instruments, Leighton Buzzard, UK) and a pH electrode (HI 1131, HANNA Instruments), which was calibrated daily.

Table 1: Solution composition and concentration of the buffered solutions.

	Solution composition / mL					
pH	0.05M	0.1M	0.1M	0.1M	0.1M	Final

	citric acid	potassium phosphate dibasic	potassium phosphate monobasic	sodium carbonate	sodium bicarbonate solution	concentration of [AH]/mM
3.0	39.8	10.2				20.0
4.0	30.0	20.0				15.0
6.0		13.0	87.0			43.5
6.3		21.0	79.0			39.5
6.75		49.0	51.0			25.5
7.5		87.0	15.0			7.5
9.2				4.0	46.0	23.0
10.4				38.5	11.5	5.75

Electrochemical Equipment

Macro-electrode experiments were performed on a glassy carbon (GC) working electrode (radius = 1.50 mm, CH instruments, TX, USA) using a computer controlled Autolab potentiostat 30 (Metrohm Auotlab B.V., Utecht, The Netherlands) using NOVA 1.0. A saturated calomel electrode (SCE, +0.242V vs SHE, ALS Co. Ltd, Tokyo, Japan) was used as the reference electrode. The three electrode cell configuration was then completed using a carbon counter electrode. Prior to use the working macro-electrode was polished on aqueous slurries of 1, 0.3, 0.05 μm alumina in descending order of size. Alumina residue was then removed from the electrode surface by rinsing with excess ultrapure water and subsequently dried under nitrogen flow.

A schematic of the thin-layer cell setup used for the opto-electrical measurements is depicted in the SI section 1. The cell used a three electrode setup, where two carbon fibres acted as the working and counter electrodes respectively and a third carbon fibre coated with a thin-layer of silver epoxy (RS Components LTd, UK) was used as a pseudo-reference electrode. Potentiostatic control and sychronisation with the camera was provided by an in-house built device, as developed previously.[25] The electrolyte solution was bubbled with N_2 gas for 20 minutes prior to transfer to the thin-layer opto-electrical cell through a capillary tube.

Micoscope and Image Analysis

The fluorescence excitation light source is provided by a LQ-HXP 120V lamp. Optical measurements were made on a Zeiss Axio Examiner. A1 Epifluorecence

microscope (Carl Zeiss Ltd., Cambridge UK) using a 20X air objective (NA = 0.5, EC Plan-Neofluar). The emission, excitation and dichromic filter set used was the MDF-FITC (Thorlabs, Ely, UK). The reflection/transmission band transition of the dichroic occurs at ~500 nm for this filter and has an excitation band of 475±17.5 nm, further details of the excitation, emission and dichroic filters can be found in the SI Section 2. Image acquisition was provided by a Hamamatsu ORCA-Flash 4.0 Digital CMOS camera (Hamamatsu, Japan), providing 16-bit images with 4 megapixel resolution. Images were acquired with an exposure time of 30.0 ms and at 10 f.p.s. Image processing and intensity extraction was performed in Zen 2 pro.

Theory and Simulation

The theoretical model considers a 'half' scheme-of-square [29] for the reduction of benzoquinone (BQ) in combination with two additional reactions:

$$PTS + H^+ = HPTS \quad \text{Reaction (6)}$$

$$A + C = 2B \quad \text{Reaction (7)}$$

as shown in SI section 3, scheme 1. Reaction (6) is the acid dissociation of HPTS and reaction (7) is the thermodynamically favorable comproportionation step to form semiquinone. While these reactions are explained in full detail in the below section `Results and Discussion', at this point we already note that the simulation provides a simplified model for the protonation and deprotonation mechanisms of the reduced BQ species through direct reaction with HPTS and PTS, respectively. Consequently all forms of BQ exclusively protonate and deprotonate via the direct reaction with PTS and HPTS. Given that there are many pathways in which the protonation of PTS and deprotonation of HPTS can take place, both were additionally enabled to change their protonation state in the absence of BQ which was assumed to be a rapid process and hence in equilibrium at any time. Depending on the position of the equilibrium, either the forward homogeneous rate constant k_f^{2nd} (i.e. B + HPTS → E +

PTS) or the backward k_b^{2nd} (i.e. E + PTS → B + HPTS) is set to the diffusional limit, which is 7.4 x 10^9 $M^{-1}s^{-1}$ in aqueous solution, the reverse reaction constant is calculated by diffusional limit/equilibrium constant.[30] Due to the high electrolyte concentration, the small size of the electrode geometry, and the short duration of the experiment, we neglect all mass transport mechanisms other than diffusion and determine concentration profiles and electrode currents on the basis of coupled reaction and diffusion equations solved subject to appropriate boundary conditions.

The resultant one-dimensional problem is solved using an explicit method for all homogeneous reactions and the backward implicit method for all mass transport and heterogeneous reactions. The extended Thomas algorithm was used to solve the linear systems of equations obtained. For further details please see SI section 3.

On the basis of the above model, we simulated the concentration profile of PTS in a chronoamperometry experiment at a cylindrical electrode as a function of electrode distance with various concentrations of protons in solution. The corresponding fluorescence intensity profiles for comparison with experimental data were determined via the numerical projection of the PTS concentration profile on a plane parallel to the electrode orientation.

Results and Discussion

This work commences by fully characterizing the redox properties of the benzoquinone/hydroquinone redox couple as a function of pH. Due to the reduction process involving the transfer of two-protons and two-electrons, seven possible intermediates exist and the exact mechanistic pathway taken for the reduction process is highly dependent upon the solution phase pH and the pK_as associated with the intermediates.[31] Consequently, to enable the voltammetric system to be accurately simulated a scheme-of-squares[29] model is constructed and validated against the experimentally recorded macro-electrode voltammetry. Having described the behavior of the p-benzoquinone/hydroquinone redox couple the

article turns to focus upon both the electrochemical and optical characterization of the fluorophore HPTS. Finally, the work concludes by studying the pH change local to the electrode and the control of the resulting reaction layer thickness by variation of the bulk proton concentration.

1,4-Benzoquinone/Hydroquinone redox couple

The reduction of p-benzoquinone (1.0mM) in a non-buffered 0.10M KCl solution was studied at a glassy carbon macroelectrode as a function of the experimental scan rate (Figure 1). A reversible redox wave is clearly observed at –0.177 V vs SCE at a scan rate of 100mVs^{-1}. Under aqueous conditions quinone reduction is generally a two electron process. [32] The first and second pK_as of reduced product hydroquinone are 9.85 and 11.4 respectively.[33] Consequently, in buffered media below pH 9 the reduction of benzoquinone (BQ) to hydroquinone (H_2BQ) is a reversible two-proton, two-electron redox process as given by the following reaction.

$$BQ + 2e^- + 2H^+ \rightleftarrows H_2BQ$$

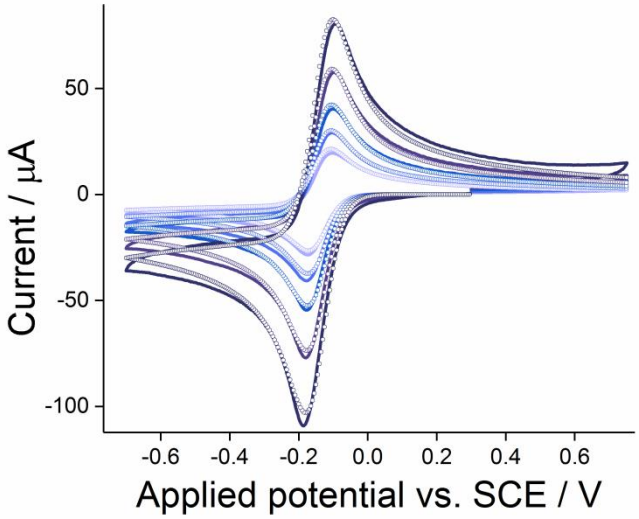

Figure 1: Cyclic voltammetry of 1.0mM 1,4-benzoquinone in a degassed aqueous solution containing 0.10M KCl. Recorded at an unmodified glassy carbon electrode with increasing scan rates of 50, 100, 200, 400 and 800 mV s^{-1} (light to dark blue).

However, in a non-buffered electrolyte (i.e. in the effective absence of protons) the reduction will *predominantly* (due to relatively high concentration of the quinone

relative to the free proton concentration) correspond overall to a two-electron reduction of the benzoquinone to the corresponding hydroquinone dianion.[33] This switch in electrochemical behavior from being a two-proton two-electron reduction to simply being a two-electron process, as a function of the proton concentration, has been experimentally reported before for the solution phase reduction of both benzoquinone and anthraquinone sulfonate derivatives.[33,34] It is important to recognize that benzoquinone is unstable in aqueous solutions more alkali than ~8 pH. This propensity to decomposition is due to the susceptibility of the structure towards undergoing rapid 1,4-Michael additions, with OH^- acting as the nucleophile. Consequently, it is only under *non-buffered* aqueous conditions that the formal potentials of the first and second electron transfer for the reduction of benzoquinone in the absence of protonation can be readily assessed.

In order to determine the diffusion coefficient of the aqueous benzoquinone the reduction was studied via both cyclic voltammetry and chronoamperometry at a platinum micro-electrode (SI section 5). Analysis of the corresponding steady-state current yields a diffusion coefficient of $1.04\pm0.05\times10^{-9}$ m^2 s^{-1}. The peak current observed in the voltammograms observed on a macroelectrode does not match that of a two electron reversible reduction. Through the use of simulation the first and second electron transfers were determined to have a formal potential of -0.12V and -0.16V vs. SCE. SI section 4 explores the simulation of this voltammetric response demonstrating why a 40 mV difference between the formal potentials of the first and second electron transfer are required. The results of this simulation data are depicted in Figure 1 where the system has been modelled as two one-electron transfers and is consistent with the following kinetic and thermodynamic parameters.

$BQ + e^- \rightleftarrows BQ^-$ $\quad$ E_f = -0.12 V vs. SCE, $k^0 \geq 0.06$ cm s^{-1}

$BQ^- + e^- \rightleftarrows BQ^{2-}$ $\quad$ E_f = -0.16 V vs. SCE, $k^0 \geq 0.06$ cm s^{-1}

Having studied the electrochemical reduction in the absence of buffer the work now continues by considering the voltammetric response of the benzoquinone in the presence of buffer.

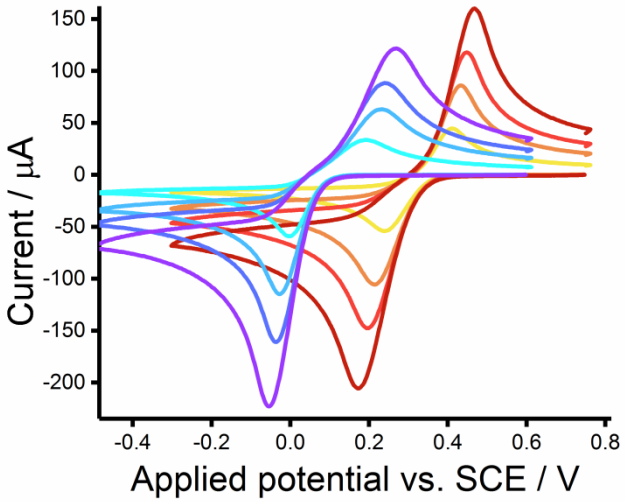

Figure 2: Cyclic voltammetric response of 2.0mM BQ in fully buffered solution with 0.10M KCl supporting electrolyte recorded on an unmodified glassy carbon electrode with increasing scan rates of 50, 200, 400 & 800 mVs^{-1}, blue to purple lines - pH 6.3 PBS, yellow to red lines - pH 2.0 HCl/KCl buffer.

Figure 2 depicts the reduction of the quinone at pH 6.3 (PBS, purple to blue lines) and pH 2.0 (HCl, red to yellow lines). First, in-part reflecting the Nernst equation in both cases the potential of the voltammetric wave occurs at a significantly more anodic potential as compared to the non-buffered voltammetric response. Second, the reduction is observed to be significantly more irreversible; the peak-to-peak separation at 100 mVs^{-1} is found to be 0.259 V and 0.219 V at pHs 6.3 and 2.0 respectively. This irreversibility reflects the alteration of the electrochemical mechanism as a function of the solution phase pH. Scheme 1 provides a summary of the known thermodynamic information regarding the benzoquinone reduction process.

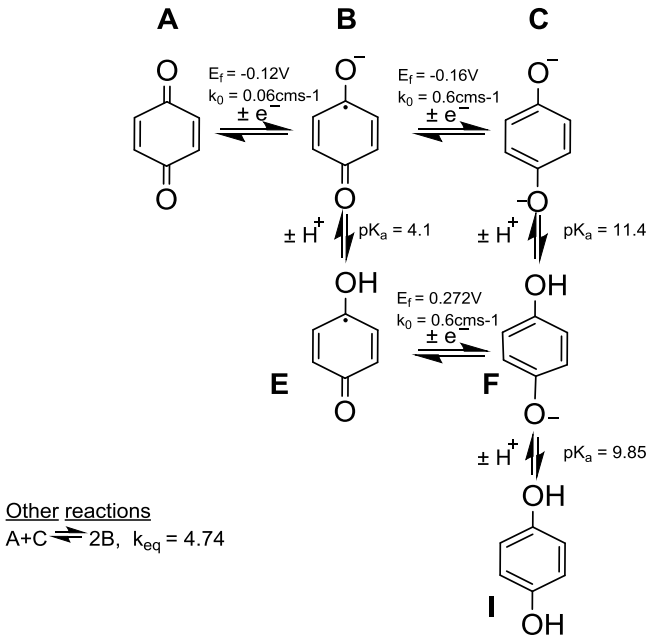

Scheme 1: Scheme of square of BQ/H_2Q redox pathway.

Here a scheme of squares has been used where electron transfers are represented as horizontal movements and proton transfers as vertical movements. This scheme includes the above reported formal potentials of the first and second electron transfer (in the absence of protonation) in combination with the literature reported pK_a values for hydroquinone (11.4 and 9.85) and the semiquinone (4.1). [35] From this thermodynamic information the formal potential for the one-electron reduction of the mono-protonated semiquinone to the hydroquinone anion can be calculated as +0.272V vs SCE. This mechanistic scheme (Scheme 1) in and of itself is sufficient to provide a physical description of the benzoquinone *reduction* process at pH 6.3. SI section 6 presents the simulated voltammetry, using Scheme 1, in comparison to the experimentally recorded response. Interestingly, although the reduction process can be broadly described using the above mechanistic pathways, the voltammetric *oxidation* of the hydroquinone is seen to occur at a significantly more negative potential than that predicted by simulation. This situation arises as in the simulation model the oxidation step becomes chemically gated by the need to deprotonate, hence as discussed in more detail in the SI section 6, it is likely that the oxidation of

the formed hydroquinone proceeds via a mechanistic route not presented in Scheme 1. This may suggest that the initial re-oxidation step proceeds via a concerted-proton-electron transfer.[36-39]However, for the present purposes the mechanism outlined above provides sufficient physical detail to enable the accurate simulation and description of the pH change local to the electrode in a chronoamperometry experiment, *vide infra*.

8-hydoxypyrene-1,3,6-trisulfonic acid (HPTS) : electrochemical characterization

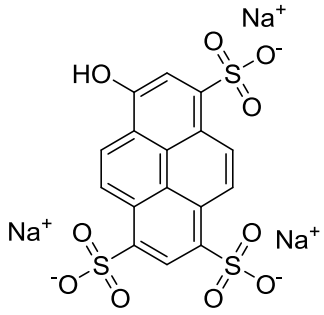

Figure 3. Chemical structure of HPTS

The voltammetric behavior of HPTS (Figure 3) was studied at a glassy carbon macroelectrode in buffered media ranging from pH 3.0-10.4. No reductive features were observed in a reductive sweep of 1mM HPTS in PBS buffer supported by 0.1M KCl from -0.5V to -1.5V, prior to cathodic solvent breakdown. As depicted in Figure 4 a reversible pH sensitive oxidative wave is observed between +0.4 to +0.65 V vs SCE. At higher potentials a second irreversible oxidative feature is observed, see SI section 7. The first reversible oxidative wave at 0.40 - 0.65 V is assigned as relating to the one-electron oxidation of the phenolic moiety, where the formed radical is likely delocalized across the pyrene structure.[40] Commonly, phenol oxidation is observed to be an irreversible process often coupled with radical dimerisation.[41] However, in the present case the oxidative product is stable on the experimental timescale (as evidenced by the voltammetric waveshape). This stability is likely due to the delocalization of the radical, and the steric and coulombic repulsion afforded by the presence of the sulfonate groups on the HPTS. The inlay of Figure 4 depicts the variation of the mid-point potential of the votlammetric feature as a function of pH.

Below ~pH 7 the peak position varies approximately linearly as a function of pH (59.0 ± 0.1 mV pH^{-1}), and above pH 7 the position of the voltammetric wave is effectively insensitive to the solution phase pH.

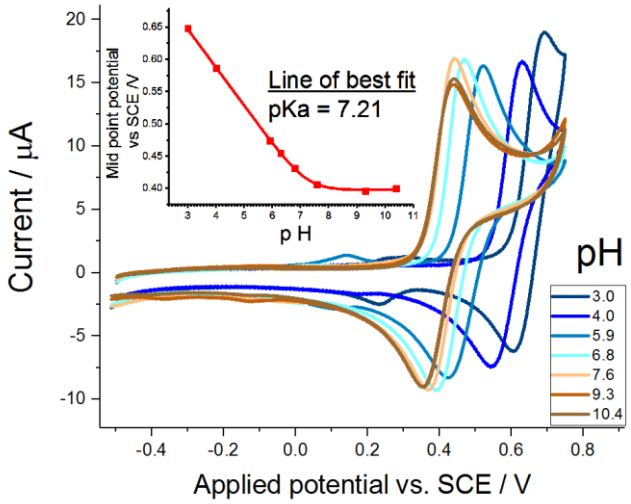

Figure 4: Cyclic voltammograms of 1.0 mM HPTS in various pH buffer solution, degassed & containing 0.10M KCl supporting electrolyte, recorded on a unmodified GC electrode at scan rates of 200mVs^{-1}. Inlay. Plot of mid-point potential vs pH, fitting function $E = E_f + RT/F * ln(1+[H^+]/K)$, where K is the acid dissociation constant.

This switch in behavior reflects the pK_a of the phenolic group and signifies the electrochemical process changing from a one-electron, one-proton oxidation (HPTS - e^- - H^+ → PTS) to a one-electron oxidation (HPTS – e^- → $HPTS^+$) above the pK_a of the alcohol. Analysis of the mid-point potential yields a direct measure of the associated pK_a in this 0.10 M KCl containing media to be 7.2±0.03.

HPTS is an example of a "photoacid",[42] where the pK_a of the phenolic group is ~0.4 in the excited state. Figure 5 shows the UV-vis absorption spectra of HPTS as a function of the solution phase pH. Below pH 7 the protonated form of the fluorophore adsorbs at 403 nm, deprotonation leads to a shift in the absorption maxima to 454 nm, with an isobectic point at 415 nm. Due to rapid deprotonation of the excited form of the fluorophore, both species exhibit a strong emission peak at 520 nm (see SI section 8).

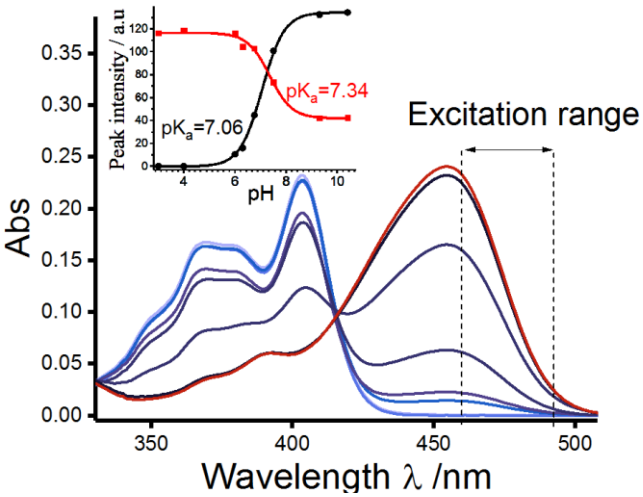

Figure 5: UV absorption spectrum of 10μM HPTS in 0.10M KCl as a function of pH. The pH values are 3.0, 4.0, 6.0, 6.3, 6.75, 7.5 & 9.3 from light blue to dark blue, red line = pH 10.4. Inlay. Plot of the fluorescence emission intensity at 520nm with the UV absorption wavelength of 403nm(red) & 454nm (black) vs pH.

The inlay of Figure 5 depicts the variation of the emission peak intensity at 520 nm as a function of pH, using two different excitation wavelengths of 454 and 403 nm. Depending upon the excitation wavelength used, a clear switch in the magnitude of the emission intensity is observed upon protonation/deprotonation of the HPTS. Following the Henderson-Hasselbach equcation, the fitting function for the 454 excitation wavelength is $y=c/(1+10^{pKa-pH})$, where c is a constant. It is this switch in fluorescence intensity as a function of pH that we use to indicate the change in the pH adjacent to the electrode surface during the course of the reduction event. In the work below an excitation band of 475±17.5 nm is used to illuminate the opto-electrochemical cell, this excitation band position is indicated on Figure 5. Hence, deprotonation of the fluorophore will lead to a significant enhancement (by factor of ~480 as estimated from Figure 5 inlay, black) of the fluorescence intensity.

Visualising the reaction layer

The reduction of benzoquinone (1.0mM) at a carbon fibre (diameter 7.0μm) wire electrode suspended in a degassed solution containing the fluorophore HPTS (2mM) and a variable proton concentration (0.0-0.14 mM) was studied in a thin layer opto-electrochemical cell. Figure 6 shows a series of representative fluorescence

microscope images for the reduction process.

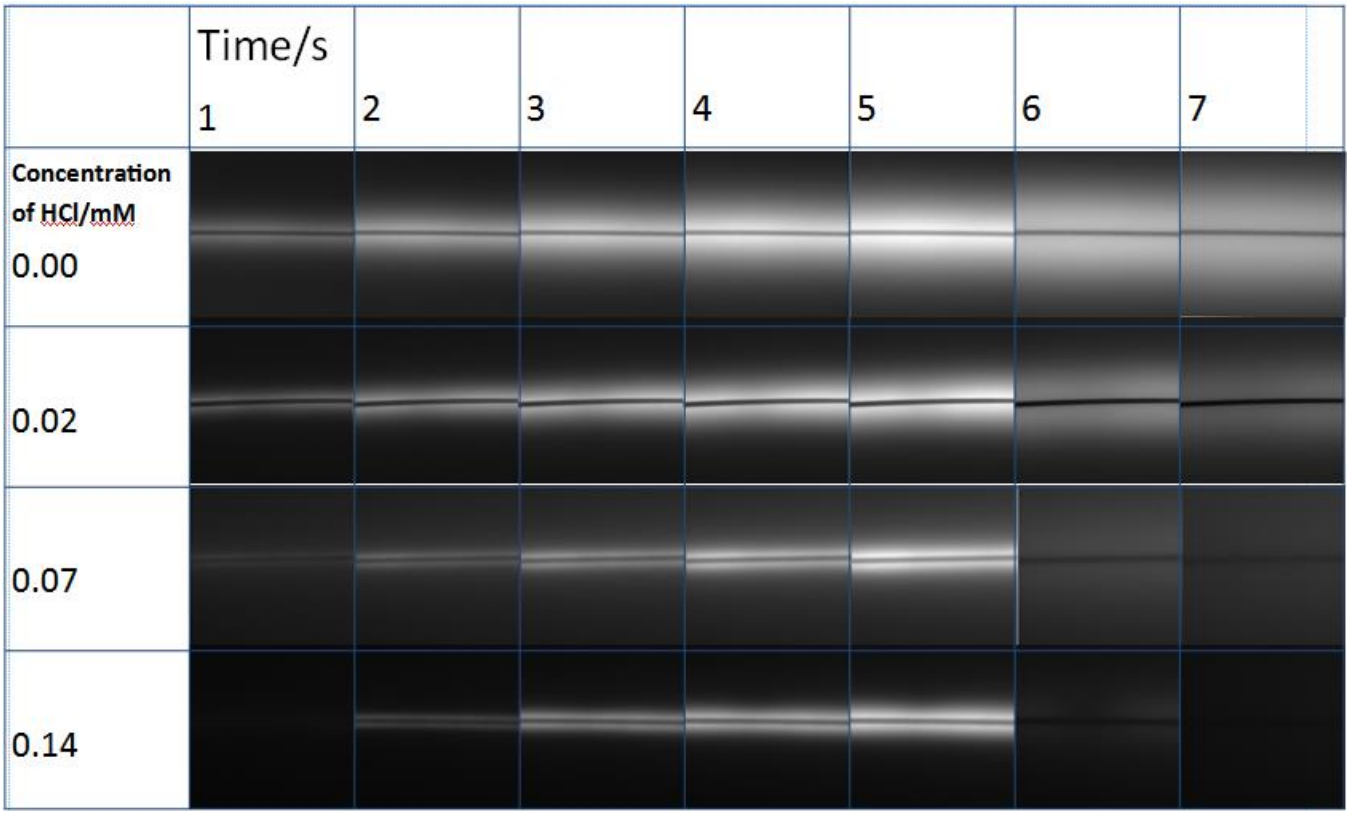

Figure 6: Fluorescence microscope images of a potentiostatically controlled carbon fibre wire electrode (diameter = 7.0µm) at a potential of -0.6V for 5 seconds followed by 0.0V for 2 seconds (potentials measured against a silver pseudo reference electrode). The solution contains 1.0mM BQ & 2.0mM HPTS and various concentration of HCl (0.00-0.14 mM), degassed. Image series shows progression of the buildup and depletion of the deprotonated fluorophore (PTS) as function of time.

Upon application of the reduction potential (-0.6 V vs Ag pseudo reference electrode) proton consumption leads to an increase in the pH adjacent to the electrode surface. This increase in pH leads to the deprotonation of the HPTS fluorophore leading to a local increase in the fluorescence intensity as a function of time. In the absence of the addition of protons to the system the proton depletion zone extends far away from the electrode surface. After 5 seconds the potential of the electrode is switched to 0.0 V (vs the pseudo reference) at a potential at which the benzoquinone reduction does not occur. Upon ceasing the reduction the intensity of the fluorescence local to the electrode decreases as the system undergoes diffusional relaxation. As can be seen from Figure 6, the addition of protons to the system serves to significantly contract *and controls* the distance over which the deprotonated fluorophore exists. Moreover,

after stopping the reduction, the fluorescence intensity rapidly decreases as the fluorophore becomes protonated.

Using the mechanistic scheme for the reduction of benzoquinone as outlined previously and by inclusion of the appropriate protonation equilibria into the scheme. The concentration profiles of the protonated and deprotonated fluorophore can be numerically predicted as a function of time, and the solution phase free proton concentration. Figure 7 depicts the variation of the simulated fluorophore concentration profile as a function of the distance away from the electrode surface in the absence of added protons and demonstrates how the profile is predicted to evolve as a function of time.

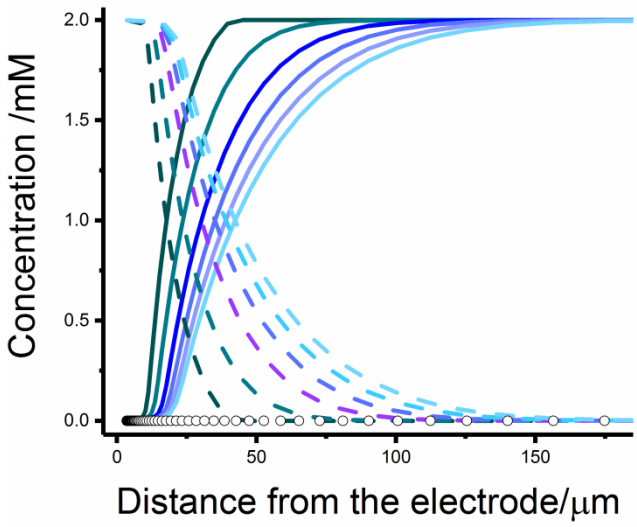

Figure 7: Simulated concentration profile with 1.0 mM BQ & 2.0 mM of HPTS on a r = 3.5μm cylindrical electrode, as a function of time with -0.6 V potential step at t = 0s. Solid line displays concentration profile of the fluorophore HPTS, dotted line represents the deprotonated fluorophore PTS and circles for protons. Time at 0.5, 1, 2, 3, 4 & 5 seconds displayed from black to light blue.

As seen from Figure 7, as the reduction proceeds, the proton depletion zone builds and the deprotonated PTS layer thickness increases. SI section 9 depicts the concentration profiles for the fluorophore in the presence of protons demonstrating the contraction of the proton depletion zone to a thin reaction layer close to the electrode surface.

The microscope images shown in Figure 6 provide not just a qualitative indication of the reaction layer thickness but through measurement of the fluorescence intensity

profile across the wire, a quantitative assessment of the (relative) local concentration profile can be obtained.

Figure 8 depicts the measured and numerically predicted fluorescence intensity profiles as a function of the lateral distance across the wire.

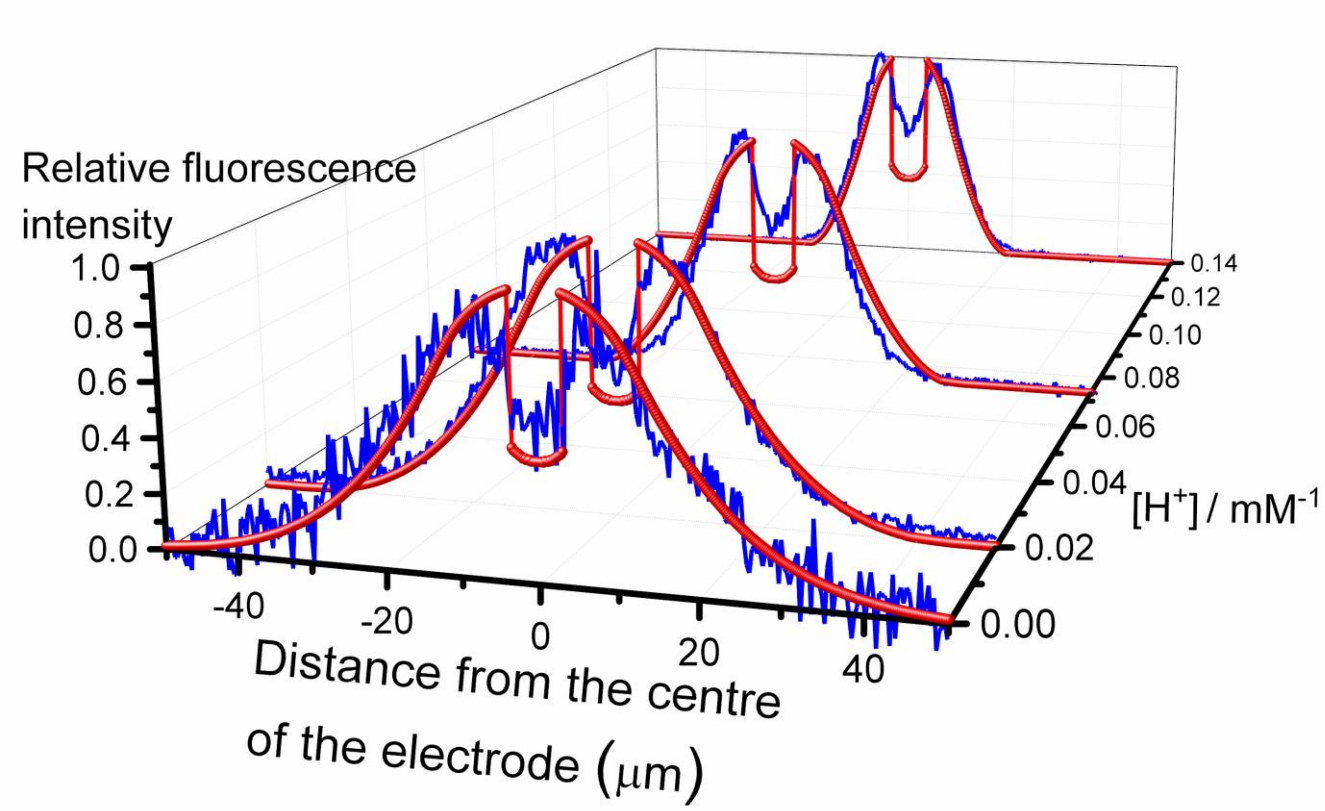

Figure 8: Relative intensity profile recorded at t=0.5s in a chronoamperometric experiment with step potential of -0.6 V vs pseudo reference electrode from t = 0 s, measured as a function of distance perpendicular to the cylindrical working electrode. The solution contains 1.0mM BQ, 2.0mM HPTS and varying concentrations of HCl, as measured from the experimental solution phase pH, degassed and supported by 0.10M KCl. Blue line – experiment, Red line – simulated intensity profile.

Conversion of the concentration profiles predicted from the numerical simulation to proportional fluorescence intensity profiles requires the numerical projection of the concentration profile on to a plane parallel to the cylindrical axis of the electrode. In the conversion, due to the relatively large length scales involved the diffraction limit of the microscope is not considered. We note that the dip in the intensity profile observable both in the experiment and simulation is likely due to the presence of

fluorophore below the opaque wire electrode that is non-observable. The numerically predicted and experimentally measured fluorescence intensity profiles shown in Figure 8 are seen to be in excellent agreement. In the absence of protons the intensity profile half maximum intensity is found to be 13.2 μM away from the electrode. The addition of 0.14 mM protons to the solution leads to the contraction of the fluorophore to a thinner reaction layer adjacent to the electrode with an associated half maximum intensity of 6.5 μm away from the electrode. This demonstrates how the spatial extent of a pH change at an electrode surface can be readily visualized and controlled.

Conclusions

The use of homogeneous reactions to dynamically control a fluorescence pH sensitive reaction layer has been successfully demonstrated by both simulation and experiment. Herein, the reduction of p-benzoquinone in the presence of the pH sensitive fluorophore HPTS has been studied in a combined opto-electrochemical cell. The electrochemically induced reduction of the quinone at the carbon electrode results in a local pH increase. This change in pH is visualized via the fluorophore, allowing the spatial extent of the proton depletion zone to be quantified. Addition of a finite proton concentration to the system allows the extent of the proton depletion zone to be controlled. Excellent agreement between the experimentally recorded and numerically predicted intensity profiles is observed.

A significant advantage of fluorescence electrochemical microscopy is its ability to rapidly visualize large areas (cf. 0.44cm^2 under this particular objective lens) without the need to form images via rastering. However, to-date the application of the technique has in part been limited by the diffusional blurring of the fluorophore, reducing the systems effective resolution dramatically. Here we demonstrate that chemically confining the fluorophore to a thin reaction layer is potentially a highly effective route to improving the systems resolution.

Supporting Information

Further information relating to following can be found in the supporting information:

- Opto-electrochemical cell design
- Theoretical model and simulation results
- Further characterisation of p-benzoquinone
- Voltammetry and fluorescence spectra of HPTS

Acknowledgements

The research leading to these results has received partial funding from the European Research Council under the European Union's Seventh Framework Programme (FP/2007-2013) / ERC Grant Agreement n. [320403].

References

(1) Molina, A.; Gonzalez, J.; Martinez-Ortiz, F.; Compton, R. G. *J. Phys. Chem. C* **2010**, *114*, 4093-4099.
(2) Nič, M.; Jirát, J.; Košata, B.; Jenkins, A.; McNaught, A. *IUPAC* **2009**.
(3) Zhan, D. P.; Han, L. H.; Zhang, J.; Shi, K.; Zhou, J. Z.; Tian, Z. W.; Tian, Z. Q. *Acc. Chem. Res.* **2016**, *49*, 2596-2604.
(4) Tian, Z. W.; Fen, Z. D.; Tian, Z. Q.; Zhuo, X. D.; Mu, J. Q.; Li, C. Z.; Lin, H. S.; Ren, B.; Xie, Z. X.; Hu, W. L. *Faraday Discuss.* **1992**, *94*, 37-44.
(5) Zhang, J.; Jia, J. C.; Han, L. H.; Yuan, Y.; Tian, Z. Q.; Tian, Z. W.; Zhan, D. P. *J. Phys. Chem. C* **2014**, *118*, 18604-18611.
(6) Ufheil, J.; Boldt, F. M.; Borsch, M.; Borgwarth, K.; Heinze, J. *Bioelectrochemistry* **2000**, *52*, 103-110.
(7) Borgwarth, K.; Heinze, J. *J. Electrochem. Soc.* **1999**, *146*, 3285-3289.
(8) Borgwarth, K.; Ricken, C.; Ebling, D. G.; Heinze, J. *Phys. Chem. Chem. Phys.* **1995**, *99*, 1421-1426.
(9) Zhang, L.; Ma, X. Z.; Zhuang, J. L.; Qiu, C. K.; Du, C. L.; Tang, J.; Tian, Z. W. *Adv. Mater.* **2007**, *19*, 3912-+.
(10) Zhan, D.; Han, L.; Zhang, J.; Shi, K.; Zhou, J. Z.; Tian, Z. W.; Tian, Z. Q. *Acc Chem Res* **2016**, *49*, 2596-2604.
(11) Patterson, M. L.; Allen, C. S. *Anal. Chem.* **1985**, *57*, 2751-2752.
(12) Engstrom, R. C.; Weber, M.; Wunder, D. J.; Burgess, R.; Winquist, S. *Anal. Chem.* **1986**, *58*, 844-848.
(13) Bard, A. J.; Fan, F. R. F.; Kwak, J.; Lev, O. *Anal. Chem.* **1989**, *61*, 132-138.
(14) Engstrom, R. C.; Ghaffari, S.; Qu, H. W. *Anal. Chem.* **1992**, *64*, 2525-2529.
(15) Fiedler, S.; Hagedom, R.; Schnelle, T.; Richter, E.; Wagner, B.; Fuhr, G. *Anal. Chem.* **1995**, *67*, 820-828.
(16) Bowyer, W. J.; Xie, J.; Engstrom, R. C. *Anal. Chem.* **1996**, *68*, 2005-2009.
(17) Vitt, J. E.; Engstrom, R. C. *Anal. Chem.* **1997**, *69*, 1070-1076.
(18) Rudd, N. C.; Cannan, S.; Bitziou, E.; Ciani, L.; Whitworth, A. L.; Unwin, P. R. *Anal. Chem.* **2005**, *77*, 6205-6217.
(19) Cannan, S.; Macklam, I. D.; Unwin, P. R. *Electrochem. Commun.* **2002**, *4*, 886-892.
(20) Colley, A. L.; Williams, C. G.; Johansson, U. D.; Newton, M. E.; Unwin, P. R.; Wilson, N. R.; Macpherson, J. V. *Anal. Chem.* **2006**, *78*, 2539-2548.
(21) Grime, J. M. A.; Edwards, M. A.; Rudd, N. C.; Unwin, P. R. *Proc. Natl. Acad. Sci. U. S. A.* **2008**, *105*, 14277-14282.
(22) Bouffier, L.; Doneux, T.; Goudeau, B.; Kuhn, A. *Anal. Chem.* **2014**, *86*, 3708-3711.
(23) Sjoback, R.; Nygren, J.; Kubista, M. *Spectrochim. Acta Mol. Biomol. Spectrosc.* **1995**, *51*, L7-L21.
(24) Rutkowska, A.; Bawazeer, T. M.; Macpherson, J. V.; Unwin, P. R. *Phys. Chem. Chem. Phys.* **2011**, *13*, 5223-5226.
(25) Batchelor-McAuley, C.; Little, C. A.; Sokolov, S. V.; Katelhon, E.; Zampardi, G.; Compton, R. G. *Anal.*

Chem. **2016**, *88*, 11213-11221.
(26) Doneux, T.; Bouffier, L.; Goudeau, B.; Arbault, S. *Anal. Chem.* **2016**, *88*, 6292-6300.
(27) Guerrette, J. P.; Percival, S. J.; Zhang, B. *J. Am. Chem. Soc.* **2013**, *135*, 855-861.
(28) Zhou, X. C.; Andoy, N. M.; Liu, G. K.; Choudhary, E.; Han, K. S.; Shen, H.; Chen, P. *Nat. Nanotechnol.* **2012**, *7*, 237-241.
(29) Jacq, J. *J. Electroanal. Chem.* **1971**, *29*, 149-180.
(30) Connors, K. A. *Chemical kinetics : the study of reaction rates in solution*; VCH: New York, N.Y., 1990.
(31) Batchelor-McAuley, C.; Li, Q.; Dapin, S. M.; Compton, R. G. *J. Phys. Chem. B* **2010**, *114*, 4094-4100.
(32) Shim, Y. B.; Park, S. M. *J. Electroanal. Chem.* **1997**, *425*, 201-207.
(33) Quan, M.; Sanchez, D.; Wasylkiw, M. F.; Smith, D. K. *J. Am. Chem. Soc.* **2007**, *129*, 12847-12856.
(34) Batchelor-McAuley, C.; Kozub, B. R.; Menshykau, D.; Compton, R. G. *J. Phys. Chem. C* **2011**, *115*, 714-718.
(35) Laviron, E. *J. Electroanal. Chem. Interfacial Electrochem.* **1984**, *164*, 213-227.
(36) Laviron, E. *J. Electroanal. Chem. Interfacial Electrochem.* **1980**, *109*, 57-67.
(37) Laviron, E. *J. Electroanal. Chem. Interfacial Electrochem.* **1981**, *124*, 1-7.
(38) Laviron, E. *J. Electroanal. Chem. Interfacial Electrochem.* **1983**, *146*, 15-36.
(39) Finklea, H. O. *J. Phys. Chem. B* **2001**, *105*, 8685-8693.
(40) Aliaga, C.; Arenas, A.; Aspee, A.; Lopez-Alaron, C.; Lissi, E. A. *Helv. Chim. Acta* **2007**, *90*, 2009-2016.
(41) Costentin, C.; Hajj, V.; Louault, C.; Robert, M.; Saveant, J. M. *J. Am. Chem. Soc.* **2011**, *133*, 19160-19167.
(42) Spry, D. B.; Goun, A.; Fayer, M. D. *J. Phys. Chem. A* **2007**, *111*, 230-237.

For Table of Contents Only.